STRONG FLUID-STRUCTURE INTERACTION EFFECTS IN SUBWAVELENGTH HELMHOLTZ RESONATORS FOR UNDERWATER ACOUSTICS: A COMPARATIVE STUDY FOR VIBROACOUSTIC DESIGN APPLICATIONS

Dario Magliacano[1], Chiara Gazzola[2], Eric Ballestero[1], Marco Miniaci[1]

[1] *Department of Structural, Building and Geotechnical Engineering, Polytechnic of Turin, Italy*
[2] *Department of Civil and Environmental Engineering, Polytechnic of Milan, Italy*

This paper is a revised version of the authors' submitted manuscript that was peer-reviewed by at least two anonymous reviewers.

Abstract

Low-frequency underwater sound absorption is challenging because large wavelengths and strong fluid-structure interaction make rigid-wall Helmholtz models only conditionally valid. This work compares 16 water-filled resonator configurations, combining four geometric sets with analytical, hard-wall, aluminum, and compliant-polymer wall models. Analytical and hard-wall predictions remain almost coincident, with frequency deviations below 1% and near-perfect absorption. Aluminum preserves high peak absorption while causing moderate, predictable downshifts of about 5-13%. In contrast, compliant polymeric walls produce strong detuning and lower peak absorption, indicating that wall compliance must be accounted for in the resonant mechanism. The results provide compact design guidelines for underwater resonators and indicate when rigid-wall approximations can still be used for preliminary vibroacoustic design.

Keywords: *underwater acoustics, Helmholtz resonator, electro-acoustic analogy, vibro-acoustics, material compliance*

1. Introduction

Helmholtz-type resonators are a standard route to sub-wavelength acoustic tuning, but their underwater use is complicated by large fluid inertia, long wavelengths, and strong fluid–structure interaction. Consequently, low-frequency waterborne absorbers often rely on compliant coatings, local resonances, quasi-Helmholtz mechanisms, ultrathin metasurfaces, or hybrid/broadband metastructures rather than purely rigid cavities [1], [2], [3], [4], [5], [6]. For water-filled cylindrical resonators, previous analytical and experimental studies have shown that wall elasticity, wall thickness, wall material, radiation impedance, and evanescent structural-acoustic effects can substantially alter the resonance of small underwater Helmholtz resonators [7], [8], [9], [10]. Against this background, the present paper provides a compact screening study for design rather than an exhaustive multiphysics optimization. In the terminology of statistical design of experiments, a screening design aims to identify the dominant factors or main effects before detailed optimization [11]. Here, this means isolating the leading influence of wall compliance by comparing four geometric sets and four wall idealizations/materials. This question is relevant to vibroacoustic pre-design, model reduction, and architected acoustic media, where compact structural-acoustic models and effective-impedance descriptions are often used for design screening [12], [13], [14], [15], [16], [17], [18]. Sixteen configurations are therefore analyzed: each geometric set is evaluated with an analytical baseline, a hard-wall baseline, aluminum walls, and plastic polymer walls.

2. Configuration set and modeling framework

2.1. Electro-acoustic description

The analyzed device is a water-filled cylindrical-neck/cylindrical-cavity resonator embedded in a square unit cell of side H, with cell surface $S = H^2$, as shown in Fig. 1.

The workflow used in this design study is based on an electro-acoustic analogy written in terms of the surface impedance

$$Z_s = SZ_c + Z_p, \tag{1}$$

Corresponding author: *dario.magliacano@polito.it, marco.miniaci@polito.it.*

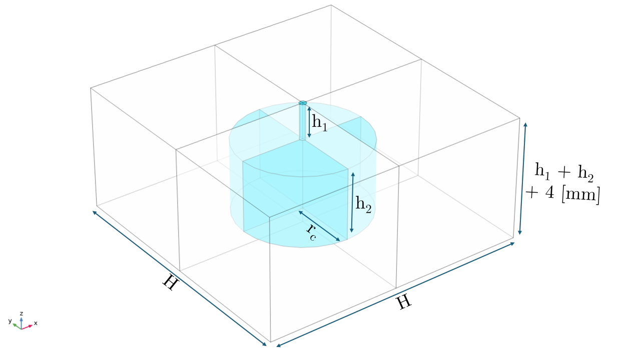

Figure 1: Example geometry of the water-filled cylindrical-neck / cylindrical-cavity resonator embedded in a square unit cell.

where Z_c is the cavity impedance and Z_p is the neck impedance. Under the low-frequency lumped-cavity approximation, namely assuming that the acoustic wavelength is much larger than the cavity dimensions and that the pressure remains nearly uniform over the cavity volume, the water-cavity impedance is approximated as

$$Z_c = -\mathrm{j}\,\frac{\rho_w c_w^2}{\omega V_w}, \tag{2}$$

with j the imaginary unit, ρ_w the water density, c_w the sound speed in water, ω the angular frequency, and V_w the cavity volume. Equation 2 is therefore used as a compact low-frequency compliance term for the water cavity, rather than as a full-wave description of the pressure field inside the resonator. The normal-incidence absorption coefficient is then obtained from the normalized impedance $z_s = Z_s/Z_0$, where $Z_0 = \rho_w c_w$ is the characteristic acoustic impedance of water, through

$$\alpha = 1 - \left|\frac{z_s - 1}{z_s + 1}\right|^2, \tag{3}$$

which also makes the impedance-matching interpretation explicit. Under normal incidence, peak absorption is obtained when the resonator surface impedance matches the characteristic impedance of water, namely when $z_s \approx 1$, or equivalently when $\Re(z_s) \approx 1$ and $\Im(z_s) \approx 0$. In a complementary complex-frequency interpretation, this corresponds to the condition in which a zero of the reflection coefficient reaches the real-frequency axis, i.e., to critical coupling between leakage and dissipation. The numerical model, implemented in COMSOL using the built-in Acoustic-Structure Boundary multiphysics coupling between "Pressure, Acoustics and Frequency Domain" and "Solid Mechanics", is discretized with 3D free tetrahedral elements, the number of which is determined through a mesh convergence analysis. The element order is Quadratic Lagrange for water domains, and Quadratic Serendipity for the solid one. The main interest of the present comparison is to quantify the effect of the selected wall model on the final tuning. Two limiting cases are therefore included: an analytic configuration based on the electro-acoustic analogy and a numerically idealized sound-hard boundary wall configuration. These are compared with two realizable materials: aluminum and a 3D-printable plastic polymer. This setup enables isolation of the role of structural compliance without altering the neck-cavity topology. It should be emphasized that this is a fixed-geometry comparison: the purpose is not to determine the best achievable polymeric design after re-optimization, but to quantify how much the same target geometry departs from the rigid-wall tuning once wall deformability is introduced. A compliant plastic polymer could, in principle, be re-tuned through a different geometry and a compliance-aware model; however, that design problem lies beyond the scope of the present screening exercise.

2.2. Post-processing indicators

In addition to the raw peak frequency and peak absorption, three derived indicators are used in the following discussion. First, the frequency shift of each material with respect to the analytical baseline of the same geometric set is defined as

$$\Delta_f = 100\,\frac{f_{\text{peak}} - f_{\text{peak}}^{(\text{an})}}{f_{\text{peak}}^{(\text{an})}}\,. \tag{4}$$

where f_{peak} denotes the peak-absorption frequency of the considered wall model, and $f_{\text{peak}}^{(\text{an})}$ denotes the peak-absorption frequency of the analytical baseline of the same geometric set. Second, the peak-absorption retention is defined as

$$R_\alpha = \frac{\alpha_{\text{peak}}}{\alpha_{\text{peak}}^{(\text{an})}}\,. \tag{5}$$

Here, α_{peak} denotes the peak absorption of the considered wall model, whereas $\alpha_{\text{peak}}^{(\text{an})}$ denotes the peak absorption of the analytical baseline of the same geometric set. R_α measures how closely a realizable wall preserves the idealized absorption level. Third, for the two realizable materials, the panel areal mass m_A is computed from the exported mass $M_{0.6\times0.8}$ of a 0.6 m × 0.8 m panel through

$$m_A = \frac{M_{0.6\times0.8}}{0.48}\,, \tag{6}$$

where 0.48 is the panel area in square meters. These indicators enable the present study to assess not only whether the resonance moves, but also whether it does so while retaining absorber efficiency and acceptable structural weight.

2.3. Analyzed configurations

Table 1 summarizes the four geometric sets. Sets 1 to 4 progressively reduce the unit-cell side, cavity radius, and cavity height. The neck height remains fixed at 10 mm, whereas the neck diameter is 3 mm for the

Table 1: Geometric sets extracted from the analyzed configuration file. Each set is repeated for the four wall idealizations/materials. Here, H is the unit-cell side, d is the neck diameter, h_1 is the neck height, r_c is the cavity radius, and h_2 is the cavity height.

Set	H [m]	d [m]	h_1 [m]	r_c [m]	h_2 [m]
1	0.136	0.003	0.010	0.043	0.050
2	0.132	0.003	0.010	0.031	0.040
3	0.103	0.003	0.010	0.023	0.030
4	0.074	0.002	0.010	0.018	0.020

first three sets and 2 mm for the smallest one. These dimensions yield cavity volumes ranging from about 2.90×10^{-4} to 2.04×10^{-5} m^3.

The corresponding frequency windows in the stored absorption curves are 200 Hz to 400 Hz for Set 1, 400 Hz to 600 Hz for Set 2, 700 Hz to 900 Hz for Set 3, and 800 Hz to 1000 Hz for Set 4. These windows were selected to bracket the expected main absorption peak of each retained design and, overall, to cover a low-frequency underwater-acoustics interval extending from approximately 100 Hz to 1 kHz. This range is not associated with a single specific platform, but it is representative of application contexts in which long acoustic wavelengths are important, including low-frequency sonar and low-frequency radiated-noise mitigation for underwater structures and vehicles [19].

3. Comparative results

3.1. Absorption spectra

Fig. 2 reports the absorption curves for the sixteen analyzed configurations, grouped into four geometric sets as detailed in Table 2. Three immediate patterns emerge. First, the analytical and hard-wall solutions remain very close in all four sets. Their peak frequencies differ by only 0.59 % to 0.89 %, and the peak absorptions range from 0.966 to 0.998. This indicates that, for the chosen geometries, the purely electro-acoustic analytical estimate already captures the dominant resonance rather well when the walls are sufficiently stiff. Second, the aluminum implementation retains a narrow, high-absorption peak, but the resonance frequency is consistently shifted downward relative to the analytical reference. The shift is strongest for the largest geometry (Set 1), where the peak moves from 326 Hz to 282 Hz, i.e. by about 13.5 %. As the resonator is miniaturized, the relative shift decreases monotonically to about 4.8 % in Set 4. This trend suggests that, within the present design family, the relative penalty of wall elasticity becomes less severe as the cavity is made smaller and stiffer. Third, the plastic polymer implementation behaves qualitatively differently within the fixed geometries considered here. Its resonance is displaced far below the analytical prediction across all sets, and its peak absorption is markedly lower. The largest set peaks near 100 Hz with $\alpha \approx 0.17$, while the smallest one peaks near 417 Hz with $\alpha \approx 0.40$. Although the

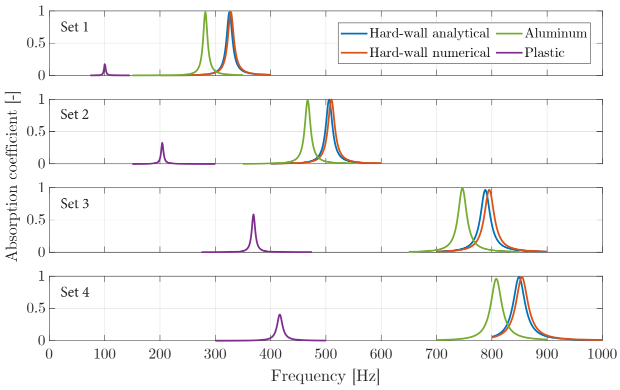

Figure 2: Normal-incidence absorption curves for the sixteen analyzed configurations, grouped into four geometric sets from top to bottom, where color groups materials. In each set, the analytical and hard-wall references are nearly coincident; aluminum introduces a moderate downshift, with high-peak absorption preserved; and the plastic polymer causes the strongest downshift, along with a pronounced reduction in peak absorption.

polymeric solution remains significantly lighter than aluminum, its compliance induces strong detuning and substantially reduces absorber effectiveness relative to the rigid-wall target. This does not imply that a polymeric concept is intrinsically unsuitable for low-frequency underwater absorption; rather, it indicates that, if such a material is selected, the geometry and the modeling assumptions should be redefined together, because the wall compliance becomes part of the resonant mechanism instead of acting as a small perturbation of the classical Helmholtz response. The same trend can be interpreted in terms of the effective normalized surface impedance introduced in Equation 3. For the analytical, hard-wall, and aluminum cases, the near-unity absorption peaks indicate that the imaginary part of z_s crosses zero near the target frequency, while the real part remains sufficiently close to the water-matching condition. The aluminum downshift is therefore mainly a change in effective reactance, with limited degradation of the resistive matching. The plastic cases are different: the resonance is displaced to much lower frequencies and the peak absorption is reduced, indicating that the surface impedance is no longer adequately matched even at the shifted peak. Since the neck-cavity geometry and the water volume are unchanged within each set, this additional detuning should not be attributed to a larger fluid mass alone. It is more consistently interpreted as a reduction of the effective stiffness, or equivalently an increase of the effective compliance, of the coupled wall-cavity system under water loading. The dense fluid activates this compliance effect, but the material-stiffness deficit governs the discrepancy between the polymeric and stiffer-wall models.

Table 2: Peak frequency and peak absorption for the four wall idealizations/materials.

Set	Conf.	Material	Peak f. [Hz]	Peak α [-]
1	1	Analytic	326	0.9816
	2	Hard wall	328	0.9863
	3	Aluminum	282	0.9838
	4	Plastic	100	0.1740
2	5	Analytic	506	0.9972
	6	Hard wall	510	0.9983
	7	Aluminum	467	0.9907
	8	Plastic	204	0.3246
3	9	Analytic	788	0.9660
	10	Hard wall	795	0.9681
	11	Aluminum	747	0.9923
	12	Plastic	369	0.5879
4	13	Analytic	849	0.9865
	14	Hard wall	854	0.9848
	15	Aluminum	808	0.9604
	16	Plastic	417	0.4044

3.2. Peak values and structural trade-offs

Table 2 condenses the peak responses and panel masses. For a panel area of 0.6 m × 0.8 m, the aluminum realizations weigh approximately 39.2 kg to 62.6 kg across the four sets, whereas the plastic polymer spans 16.7 kg to 26.7 kg. Hence, the polymeric option is much lighter, but this gain is accompanied by a drastic resonance downshift and, in three out of four sets, by a severe loss of peak absorption.

3.3. Derived design indicators

To make the trends more explicit, Table 3 reports only the derived indicators for the two realizable wall materials. Two points are especially relevant. For aluminum, the absorption-retention factor remains very close to unity in all four sets, ranging from 0.974 to 1.027. In other words, the main effect of the metallic wall is a tuning correction rather than a degradation of the absorption maximum. The frequency correction is non-negligible but bounded and monotonic across the four sets. This is a favorable design scenario because it can, in principle, be compensated by a one-shot retuning of the cavity geometry. For the plastic polymer, the situation is different. The frequency downshift is accompanied by a marked decrease in R_α, which drops to 0.177 in Set 1 and remains below 0.61 even in Set 3, the best of the four cases. The polymeric wall, therefore, acts as a coupled compliant subsystem rather than as a nearly rigid container. From a simulation standpoint, this means that a rigid-cavity Helmholtz estimate can still serve as a useful first predictor for metal designs. In contrast, it serves only as a loose upper bound for the polymeric cases.

A second design-level observation concerns miniaturization. Across Sets 1 to 4, the characteristic unit-cell size and cavity volume are progressively reduced, but

Table 3: Derived indicators for the two realizable wall materials. R_α denotes peak-absorption retention with respect to the analytical baseline of the same set, and m_A is the areal mass extrapolated from the 0.6 m × 0.8 m panel.

Set	Material	Δ_f [%]	R_α [-]	m_A [kg/m^2]
1	Aluminum	-13.5	1.002	130.4
1	Plastic	-69.3	0.177	55.5
2	Aluminum	-7.7	0.993	127.1
2	Plastic	-59.7	0.326	54.1
3	Aluminum	-5.2	1.027	106.1
3	Plastic	-53.2	0.609	45.2
4	Aluminum	-4.8	0.974	81.7
4	Plastic	-50.9	0.410	34.8

the realizable metallic design becomes less sensitive to wall elasticity. This indicates that the chosen geometry family approaches a more favorable stiffness-to-fluid-loading balance as it is compacted. The trend is encouraging for modeling and optimization, as it suggests that compact underwater resonators in the upper part of the present frequency range are more robust to material-induced detuning than their larger, lower-frequency counterparts.

4. Discussion

From a modeling perspective, the most relevant conclusion is that the choice of wall model is not a minor correction in underwater applications. The excellent agreement between the analytical and hard-wall results indicates that the retained electro-acoustic formulation is internally consistent and that the rigid-wall assumption is acceptable only when the structure is indeed very stiff. However, once a realizable wall material is introduced, tuning can change substantially even if the neck and cavity dimensions remain unchanged. The aluminum cases suggest a favorable compromise for compact absorbers: they stay close enough to the analytical target to preserve the intended operating band, while maintaining peak absorptions near unity. The relative downshift decreases from Set 1 to Set 4, which is useful for design, as it implies that compact cells are less sensitive to this compliance effect. In practice, this means that an analytical target around 800 Hz to 850 Hz can still be approached reasonably well with aluminum, whereas a lower analytical target around 300 Hz to 500 Hz experiences a stronger deviation if the same material family and neck concept are retained. In this sense, aluminum primarily serves as a perturbative correction to the rigid-wall model: it shifts the resonance but does not fundamentally alter the impedance-matching logic of the classical Helmholtz design. The plastic polymer cases point to the opposite limit. They are not simply shifted replicas of the rigid-wall response; they are both detuned and weakened when the same geometry is retained. This behavior is consistent with the wider literature on underwater absorbers, where low-frequency performance is often achieved precisely by exploiting compliant coatings, hybrid resonant layouts, or quasi-Helmholtz mechanisms rather than by enforcing nominally rigid cavities [3], [4], [5], [6]. In that broader sense, the polymer should not be interpreted as an intrinsically poor material choice. On the contrary, its higher compliance and damping may be advantageous if the resonator is redesigned to restore impedance matching with a material-aware geometry. The present results support a narrower conclusion: within the fixed neck-cavity topologies examined here and relative to a rigid-wall analytical target, the polymeric wall does not behave as a small correction, but as a coupled compliant subsystem. Therefore, the drawback is not merely the use of a different material per se; it is the mismatch between a rigid-wall target design and a wall model whose deformability materially alters the resonance mechanism. The comparison also clarifies the practical meaning of the two idealized references. The analytic solution is useful as a direct design law, whereas the hard-wall solution acts as a numerical rigid-wall check. Their close agreement means that the residual discrepancies seen in the realizable walls are not numerical artifacts of the post-processing workflow but rather genuine consequences of wall compliance. These observations suggest a pragmatic modeling strategy for pre-design. First, an analytical or hard-wall model can be used to quickly position the target resonance. Second, once a material candidate is selected, the tuning should be corrected using a material-aware model before the geometry is frozen. Third, if a lightweight polymeric concept is selected, one should no longer expect the rigid-wall tuning law to remain predictive; instead, the polymer compliance should be treated as a design variable in its own right and combined with geometric re-tuning to recover the desired impedance condition. This last point opens the way toward intentionally compliant or hybrid concepts, in which wall deformability is not a parasitic effect but part of the absorber design logic. These unit-cell trends also have a direct interpretation at the metasurface or structured-panel level. In subwavelength periodic panels, each resonator acts as a local impedance-controlling cell, while the large-scale absorption response depends on how such cells are distributed, repeated, or combined into supercells. From this perspective, the present results indicate that aluminum-based cells are better suited to array designs that aim to preserve a prescribed Helmholtz-type tuning with limited correction, whereas compliant polymeric cells are more naturally associated with intentionally hybrid or broadband concepts, for which geometry, material, and coupling must be optimized jointly at the panel level. The selected frequency interval also clarifies the application-level interpretation of the material choice. The hard-wall model should be regarded primarily as an ideal reference or upper-bound tuning law, rather than as a realizable material solution. Aluminum is appropriate when the design objective is a robust, relatively narrowband unit cell whose resonance must remain close to a prescribed Helmholtz-type target, for example in structured panels where each cell is assigned a specific operating frequency. By contrast, polymeric or coated concepts are more attractive when mass reduction, added damping, manufacturability, or broader-band behavior is prioritized, provided that the geometry is re-optimized to include wall compliance in the model.

5. Conclusions

A compact set of sixteen underwater Helmholtz-resonator configurations has been analyzed to quantify the effect of wall material on the tuning of normal-incidence absorption. The main findings are as follows: (i) the analytical and hard-wall references are almost indistinguishable for all four geometric sets, with resonance-frequency differences below 1% and peak absorptions close to unity; (ii) aluminum introduces a systematic but moderate downshift of the resonance frequency, from about 13.5% in the largest cell to about 4.8% in the smallest one, while preserving peak absorption between 0.96 and 0.99; within the fixed geometries examined here, the plastic polymer produces a much stronger compliance effect, reducing the resonance frequency to roughly 31-49% of the analytical reference and limiting the peak absorption to 0.17-0.59; (iv) for a 0.6 m × 0.8 m panel, aluminum remains considerably heavier than the plastic polymer, but it is also dynamically far more faithful to the intended Helmholtz tuning. Overall, the results show that material compliance is a first-order design variable for compact underwater resonators. Within the analyzed family, aluminum is the most credible realizable option when the goal is to preserve the behavior of a classical water-filled Helmholtz absorber over a prescribed low-frequency band. In contrast, a compliant polymeric wall requires a different modeling approach and, most likely, a joint redefinition of geometry and material to incorporate wall deformability into the resonant concept rather than treating it as an unwanted perturbation of the rigid-wall design. At the application level, the present unit-cell screening can be interpreted as a pre-design step for structured underwater panels and metasurfaces, where local impedance, mass, bandwidth, and robustness must be balanced before committing to full-scale optimization. Future work should therefore address compliance-aware retuning of lightweight polymeric resonators to determine whether their lower mass and higher damping can be converted into a competitive low-frequency underwater design advantage. In addition, it should extend the present screening to damping identification and experimental validation for the selected prototypes.

6. Acknowledgments

This project is supported by the European Research Council (ERC) under the European Union's Horizon Europe research and innovation programme (POSEIDON, Grant Agreement No. 101039576).
M.M. acknowledges the DREAM project that received

funding from the European Union Next-GenerationEU (National Recovery and Resilience Plan – NRRP, Mission 4, Component 2, Investment 1.2).

References

[1] E. Dong, P. Cao, J. Zhang, S. Zhang, N. X. Fang, and Y. Zhang, "Underwater acoustic metamaterials," *National Science Review*, vol. 10, no. 6, nwac246, 2023. DOI: 10.1093/nsr/nwac246.

[2] Z. Zhu et al., "A review of underwater acoustic metamaterials for underwater acoustic equipment," *Frontiers in Physics*, vol. 10, p. 1 068 833, 2022. DOI: 10.3389/fphy.2022.1068833.

[3] M. Duan, C. Yu, F. Xin, and T. J. Lu, "Tunable underwater acoustic metamaterials via quasi-Helmholtz resonance: From low-frequency to ultra-broadband," *Applied Physics Letters*, vol. 118, no. 7, p. 071 904, 2021. DOI: 10.1063/5.0028135.

[4] M. Duan, C. Yu, F. Xin, and T. J. Lu, "Deep subwavelength hybrid metamaterial for low-frequency underwater sound absorption by quasi-Helmholtz resonance," *AIP Advances*, vol. 13, no. 2, p. 025 352, 2023. DOI: 10.1063/5.0131820.

[5] H. Yang, H. Zhao, J. Yin, and J. Wen, "Hybrid meta-structure for broadband waterborne sound absorption," *AIP Advances*, vol. 9, no. 12, p. 125 226, 2019. DOI: 10.1063/1.5126807.

[6] Z. Wang, Y. Huang, X. Zhang, L. Li, M. Chen, and D. Fang, "Broadband underwater sound absorbing structure with gradient cavity shaped polyurethane composite array supported by carbon fiber honeycomb," *Journal of Sound and Vibration*, vol. 479, p. 115 375, 2020. DOI: 10.1016/j.jsv.2020.115375.

[7] Z.-F. Wang, Y.-M. Hu, Z. Meng, and M. Ni, "Acoustic characteristics of underwater cylindrical Helmholtz resonator," *Acta Physica Sinica*, vol. 57, no. 11, pp. 7022–7029, 2008. DOI: 10.7498/aps.57.7022.

[8] Z.-F. Wang, Y.-M. Hu, H. Luo, Z. Meng, M. Ni, and S.-D. Xiong, "Influence of cavity wall elasticity on resonant frequency of small underwater cylindrical Helmholtz resonator," *Acta Physica Sinica*, vol. 58, no. 4, pp. 2507–2512, 2009. DOI: 10.7498/aps.58.2507.

[9] Y.-J. Sang, Y. Lan, and Y.-W. Ding, "Study on elastic-wall fluid cavity resonant frequency of Helmholtz underwater acoustic transducer," *Acta Physica Sinica*, vol. 65, no. 2, p. 024 301, 2016. DOI: 10.7498/aps.65.024301.

[10] M. Oblak, M. Pirnat, and M. Boltežar, "Modal-interaction approach to the strong structural-acoustic coupling of an elastic Helmholtz resonator and an acoustic cavity containing a heavy fluid," *Journal of Sound and Vibration*, vol. 535, p. 117 120, 2022. DOI: 10.1016/j.jsv.2022.117120.

[11] NIST/SEMATECH, *Screening designs*, e-Handbook of Statistical Methods, 2013.

[12] M. Filippi, D. Magliacano, M. Petrolo, and E. Carrera, "Variable-kinematics finite elements for propagation analyses of two-dimensional waveguides," in *30th AIAA/CEAS Aeroacoustics Conference*, Rome, Italy, 2024. DOI: 10.2514/6.2024-3078.

[13] M. Filippi, D. Magliacano, M. Petrolo, and E. Carrera, "Wave propagation in pre-stressed structures with geometric nonlinearities through Carrera Unified Formulation," in *30th AIAA/CEAS Aeroacoustics Conference*, Rome, Italy, 2024. DOI: 10.2514/6.2024-3028.

[14] D. Magliacano, "High-order vibroacoustic modal analysis framework for fluid-structure coupling," *Aerospace*, vol. 12, no. 11, p. 994, 2025. DOI: 10.3390/aerospace12110994.

[15] M. Miniaci, A. Krushynska, A. B. Movchan, F. Bosia, and N. M. Pugno, "Spider web-inspired acoustic metamaterials," *Applied Physics Letters*, vol. 109, no. 7, p. 071 905, 2016. DOI: 10.1063/1.4961307.

[16] C. Gazzola, S. Caverni, and A. Corigliano, "From mechanics to acoustics: Critical assessment of a robust metamaterial for acoustic insulation application," *Applied Acoustics*, vol. 183, p. 108 311, 2021. DOI: 10.1016/j.apacoust.2021.108311.

[17] C. Gazzola, S. Caverni, and A. Corigliano, "Design and modeling of a periodic single-phase sandwich panel for acoustic insulation applications," *Frontiers in Materials*, vol. 9, p. 1 005 615, 2022. DOI: 10.3389/fmats.2022.1005615.

[18] E. Ballestero et al., "Scattering evaluation of equivalent surface impedances of acoustic metamaterials in large FDTD volumes using RLC circuit modelling," *Applied Sciences*, vol. 11, no. 17, p. 8084, 2021. DOI: 10.3390/app11178084.

[19] Discovery of Sound in the Sea, *Tutorial: Sonar source*, 2024.